Biochemical Journal (2020) **477** 3147–3165
https://doi.org/10.1042/BCJ20200499

PORTLAND PRESS

Research Article

Pro4 prolyl peptide bond isomerization in human galectin-7 modulates the monomer-dimer equilibrum to affect function

Michelle C. Miller[1], Irina V. Nesmelova[1,*], Vladimir A. Daragan[1], Hans Ippel[1,2], Malwina Michalak[3], Aurelio Dregni[1], Herbert Kaltner[4], Jürgen Kopitz[3], Hans-Joachim Gabius[4] and Kevin H. Mayo[1]

[1]Department of Biochemistry, Molecular Biology and Biophysics, University of Minnesota, Minneapolis, MN 55455 U.S.A.; [2]Department of Biochemistry, CARIM, University of Maastricht, Maastricht, The Netherlands; [3]Department of Applied Tumor Biology, Institute of Pathology, Medical School of the Ruprecht-Karls-University Heidelberg, Heidelberg, Germany; [4]Institute of Physiological Chemistry, Faculty of Veterinary Medicine, Ludwig-Maximillians-University Munich, Munich, Germany

Correspondence: Kevin H. Mayo (mayox001@umn.edu)

Human galectin-7 (Gal-7; also termed p53-induced gene 1 product) is a multifunctional effector by productive pairing with distinct glycoconjugates and protein counter-receptors in the cytoplasm and nucleus, as well as on the cell surface. Its structural analysis by NMR spectroscopy detected doubling of a set of particular resonances, an indicator of Gal-7 existing in two conformational states in slow exchange on the chemical shift time scale. Structural positioning of this set of amino acids around the P4 residue and loss of this phenomenon in the bioactive P4L mutant indicated *cis–trans* isomerization at this site. Respective resonance assignments confirmed our proposal of two Gal-7 conformers. Mapping hydrogen bonds and considering van der Waals interactions in molecular dynamics simulations revealed a structural difference for the N-terminal peptide, with the *trans*-state being more exposed to solvent and more mobile than the *cis*-state. Affinity for lactose or glycan-inhibitable neuroblastoma cell surface contact formation was not affected, because both conformers associated with an overall increase in order parameters (S^2). At low μM concentrations, homodimer dissociation is more favored for the *cis*-state of the protein than its *trans*-state. These findings give direction to mapping binding sites for protein counter-receptors of Gal-7, such as Bcl-2, JNK1, p53 or Smad3, and to run functional assays at low concentration to test the hypothesis that this isomerization process provides a (patho)physiologically important molecular switch for Gal-7.

Introduction

Screening for up- or down-regulation of expression of distinct genes upon changing a specific parameter is a robust approach to identify key aspects of the cascade leading to a triggered cellular response. When monitoring the impact of viral transformation (by SV40 of human keratinocytes), chemical carcinogenesis (by 7,12-dimethylbenz[a]anthracene on rat mammary carcinomas) and induction of p53 (in human colon adenocarcinoma (DLD-1) cells), a marked effect was noted for expression of a gene/protein assigned to the family of galectins, i.e. galectin-7 (Gal-7) [1–3]. In fact, due to its conspicuous up-regulation, it has even been referred to also as p53-induced gene 1 product [3]. These *ga*(lactose-binding)*lectins* are multifunctional proteins that have first been delineated to serve as molecular bridge by binding to β-galactoside epitopes of glycan chains of cellular glycoconjugates and then to mediate a wide variety of cellular activities by this functional pairing [4–8]. Beyond this role as 'readers' and 'interpreters' of glycan-based signals within the concept of the sugar code [9,10], galectins also target peptide motifs, among them distinct cytoplasmic and nuclear proteins [11,12]. The common absence of a signal peptide allows galectins to gain access to the cytoplasm, and transport mechanisms ensure

*Present address: Department of Physics and Optical Science, University of North Carolina at Charlotte, Charlotte, NC 28223 USA.

Received: 24 June 2020
Revised: 3 August 2020
Accepted: 6 August 2020

Accepted Manuscript online: 7 August 2020
Version of Record published: 4 September 2020

Biochemical Journal (2020) 477 3147–3165
https://doi.org/10.1042/BCJ20200499

routing to the nucleus or their non-classical secretion [13–17]. Indeed, immunohistochemical studies show such a distribution profile for Gal-7 in cells and tissues (for examples, please see [18–20]). As take-home message, galectins form a versatile platform for recognition processes for different types of ligands.

Functionally, Gal-7 is intimately involved in growth regulation, as illustrated, for example, by the response to ectopic expression in UV-exposed keratinocytes or in the mentioned DLD-1 tumor cells [18,21,22]. Toward this end, either glycans (as cell surface counter-receptors) [23,24], binding partners intracellularly upstream of JNK activation, or even products of Gal-7-dependent modulation of gene expression [18], come into play. Broadening its activity profile, pro-tumoral effector mechanisms have also been documented, highlighting the context-dependent nature of the outcome of the presence of Gal-7 [25,26]. Since the list of proteins that are intracellular binding partners has remarkably grown over the years, now including such potent effectors as the transcription factor Smad3 [27], p53 [28], Bcl-2 [29], E-cadherin [30] and JNK1 [31], elucidating the structural aspects of these interactions has become an important issue. Toward this end, structural characterization of Gal-7 in solution is imperative.

Having reported NMR-spectroscopical assignments [32] and initial binding studies with the canonical ligand lactose [33], we observed unexplained pairs of resonances that intrigued us. Here, we can attribute these pairs to *cis/trans* isomerization indirectly by engineering and processing a loss-of-function mutant (i.e. P4L) and directly by making specific resonance assignments for each isomer state. The *cis/trans*-states differ in the presentation of the N-terminal section which profoundly affects its local vicinity. Furthermore, the monomeric state of Gal-7 is promoted at low μM protein concentrations when P4 is in its *cis*-state. In contrast, the lactose binding-induced overall gain in conformational entropy is not affected by P4 isomerization.

Experimental

Galectin engineering, production and isotopic labeling

Primer design was based on the sequence from Genbank Accession No. NM_002307.3, the sense primer for wild-type Gal-7 was 5′-CGCTAGCATATGTCCAACGTCCCCCACAAG-3′ (*NdeI* restriction site underlined), the sense primer for the single-site Gal-7 mutant P4L 5′-CGCTAGCATATGTCCAACGTCC**T**CCACAAG-3′ (*NdeI* restriction site underlined, changed nucleotide in bold), the antisense primer in both cases was 5′-CGTACGAAGCTTTCAGAAG-ATCCTCACGGA-3′ (*HindIII* restriction site underlined). For PCR amplification, a pQE-60/Gal-7 plasmid was used as a template [18], the respective PCR products were ligated in-frame into the pET-24a (Novagen®, Sigma–Aldrich, Munich, Germany) expression vector linearized by *NdeI*/*HindIII* directing protein generation in the *Escherichia coli* strain RosettaBlue^{TM}(DE3)pLys S (Novagen®). Optimal yields of protein (wild-type Gal-7 ≈ 100–110 mg/l, for Gal-7 mutant P4L ≈ 80–90 mg/l of culture medium) were obtained in a two-step procedure using first LB medium (Roth, Karlsruhe, Germany) containing 100 μM isopropyl-β-D-thiogalactoside (IPTG) at 37°C overnight, then (with resuspended bacterial pellets) M9 minimal medium (enriched with [^{15}N]NH_4Cl and/or U-[^{13}C]glucose as medium additive(s)) and induction with 200 μM IPTG at 37°C for 16 h. The suspensions were centrifugated, and cells were lysed by the freeze–thaw approach using 7 ml of buffer (20 mM phosphate-buffered saline, pH 7.2, containing 2 mM EDTA and 4 mM β-mercaptoethanol) per gram wet cell paste. After centrifugation to pellet debris, the supernatant was fractionated by affinity chromatography on home-made lactosylated Sepharose 4B as a crucial step of purification, using buffer with 0.1 M lactose for elution, removing the sugar by several rounds of ultrafiltration and a final gel filtration, and the proteins were checked for purity and activity as previously described [23].

NMR spectroscopy

NMR experiments

NMR spectra were measured on a Varian Unity Inova 800 MHz spectrometer equipped with a triple-resonance probe and *x*/*y*/*z* triple-axis gradient unit. Sequence-specific resonance assignments have been performed using a standard set of 3D NMR experiments, as described previously [34]. Interproton distance restraints were derived from NOEs assigned in 3D ^{15}N-edited or ^{13}C-edited NOESY spectra, obtained at mixing time of 150 ms. Hydrogen bond constraints were identified from the pattern of sequential and interstrand NOEs involving NH and $C_\alpha H$ protons, and with evidence of slow amide proton-solvent (D_2O) exchange, monitored with a series of 2D ^{1}H–^{15}N HSQC experiments. NMR spectra were processed using NMRPIPE [35] and visualized using NMRVIEW [36].

NMR residual dipolar couplings

A Gal-7 sample was prepared in a liquid crystalline phase at 7.5 mg/ml of 3 : 1 14-O-PC : 6-O-PC bicelles in 20 mM potassium phosphate, pH 6.5. Lipids have been purchased from Avanti Polar Lipids, Inc. Changes in splitting relative to the isotropic $^{1}J_{NH}$ values were measured at 800 MHz on ^{15}N-labeled Gal-7 at 30°C by using in-phase anti-phase (IPAP) [^{1}H,^{15}N]-HSQC experiments [37].

NMR chemical shifts

To determine chemical shifts, ^{13}C-filtered proton spectra were acquired with a resolution of 0.5 Hz. Chemical shifts were expressed in absolute frequency with no internal reference. Chemical shifts of amide ^{15}N and ^{1}H were measured from 2D ^{1}H–^{15}N HSQC, referenced against water resonance.

NH temperature factors were determined by acquiring ^{15}N–^{1}H HSQC spectra as a function of temperature and plotting ^{1}H chemical shifts vs. the inverse temperature. The normally negative slopes of these curves provide temperature factors (units of ppb/K) that then suggest presence of hydrogen bonds when the value is relatively small.

NMR relaxation experiments

^{15}N longitudinal [$R_N(N_Z)$] and transverse [$R_N(N_X)$] relaxation terms and heteronuclear NOE enhancements were determined for lactose-loaded and -free ^{15}N-enriched Gal-7. Data were acquired at ^{1}H frequencies of 600 and 800 MHz essentially, as described previously [40–42]. $R_N(N_Z)$ and $R_N(N_X)$ were derived by fitting data collected with different relaxation delays to a single exponential decay function, and errors were determined by repeating single data points as we described earlier. Two sets of spectra were recorded for steady-state NOE intensities, one with 3-s proton saturation to achieve steady-state intensities and the other as a control spectrum with no saturation to obtain the initial intensity. NOE enhancements were calculated from the ratios of these intensities. Data for each Gal-7 state (lactose free and loaded) were analyzed using the Lipari–Szabo model free approach [43].

NMR structure calculations

Initial structures were calculated using the program XPLOR-NIH [49]. Starting with random co-ordinates, simulated annealing was carried out based on NOE distance restraints, dihedral angles, carbon chemical shifts and residual dipolar coupling (RDC) restraints using XPLOR-NIH protocols. Distance restraints were grouped into three ranges: 1.8–2.9 Å (strong), 1.8–3.3 Å (medium) and 1.8–5.0 Å (weak). For each hydrogen bond identified, two distance constraints were used: 1.6–2.4 Å for H–O constraints and 2.6–3.4 Å for N–O constraints. A total of 100 random structures were subjected to 24 k simulated annealing and cooling steps of 0.005 ps. From these structures, ten energy-minimized structures were selected based on the absence of NOE violations greater than 0.2 Å, dihedral angle violations greater than 5° and residual dipolar constants greater than 0.5 Hz.

The HADDOCK 2.0 program [50] was used to perform simultaneous docking of two lactose molecules to the Gal-7 homodimer. Based on NOEs between lactose and Gal-7, chemical shift changes induced by lactose binding and solvent-accessibility calculations, amino acid residues were set as active or passive. NOE distance restraints between Gal-7 and lactose were used as unambiguous restraints. Amino acid residues at the interface allowed switching between active and passive residues ±2 sequential residues. The docking procedure was performed in three steps using default parameters in HADDOCK and symmetry restraints with force constants equal to 300 kcal/mol: (1) randomization and rigid body energy minimization, (2) semi-flexible simulated annealing and (3) flexible explicit solvent refinement. Initially, 1000 structures were generated in the rigid body docking, and subsequently, the 100 best structures were selected for further semi-flexible simulated annealing, and then for the final refinement in the presence of explicit water. To produce final structures, we refined the minimum energy-minimized structures for lactose-loaded and -free Gal-7 in explicit solvent using the program NAMD2.6 [51].

NMR diffusion coefficients

Diffusion coefficients were measured on a Varian Unity Inova 600 MHz spectrometer equipped with an H/C/N triple-resonance probe and *x*/*y*/*z* triple-axis pulse field gradient unit. The maximum magnitude of the gradient, *g*, was calibrated using Varian deuterated water standard. Measurements were performed, as described before

Biochemical Journal (2020) 477 3147–3165
https://doi.org/10.1042/BCJ20200499

[38,39]. The value of the diffusion coefficient was estimated from the diffusion attenuation of spin-echo by using eqn (1).

$$A(g^2) = A(0)\exp\,(-\gamma^2\delta^2 g^2 D t_d), \quad (1)$$

where γ is the gyromagnetic ratio for protons, δ is the duration of the pulsed field gradient and t_d is the diffusion time, which comprises all time delays between pulses, during which the magnetization is aligned along z-axis.

Mass spectrometry

Matrix-assisted laser desorption/ionization (MALDI) time-of-flight (TOF) mass spectrometry was applied for molecular mass determination and peptide mass fingerprinting using trypsin, as previously described [44,45]. Each protein sample was dissolved in water to a final concentration of 4 μg/μl. For molecular mass determination with sinapinic acid (SA) as matrix, the protein-containing sample was further diluted with 0.1% trifluoroacetic acid (TFA) (1:5, v/v). 0.5 μl of a saturated solution of SA in ethanol was pipetted on individual spots of the MALDI target. After drying, 1 μl of protein solution was added on top of the thin SA layer, immediately followed by 1 μl of a saturated solution of SA in 0.1% TFA with 30% acetonitrile (TA30). For peptide fingerprinting, the protein (10 μg in 10 μl 40 mM NH_4HCO_3) was first treated with 2 μl of a 10 mM solution of dithiothreitol (DTT) in 40 mM NH_4HCO_3 at 45°C for 1 h to completely reduce disulfide bonds. The thiol groups were then alkylated by addition of 1 μl of a solution of 55 mM iodoacetamide in 40 mM NH_4HCO_3 at 25°C for 30 min and after adding 2.5 μl 10 mM DTT, the mixture was incubated for 15 min at 37°C to let all iodoacetamide react with the thiol group.

Tryptic digestion was performed with 100 ng trypsin in 40 mM NH_4HCO_3 solution overnight at 37°C. Digest mixtures were desalted with reversed phase ZipTip$_{C\text{-}18}$. ZipTip$_{C18}$ pipette tips were wetted three times with 10 μl TA50 (50% acetonitrile in 0.1% TFA), followed by three washes with 10 μl 0.1% TFA. Peptides were then adsorbed onto the tip by repeatedly drawing the sample solution through the ZipTip, followed by three washes with 0.1% TFA to remove salts. Sample was eluted with 2 μl of a saturated solution of α-cyano-4-hydroxy-cinnamic acid in TA50 and directly spotted on the MALDI target. All matrices were obtained from Bruker Daltonik (Bremen, Germany). Spotted samples were dried at ambient temperature prior to mass spectrometric analysis. MALDI mass spectra were collected on an Ultraflex™ TOFTOF I instrument (Bruker Daltonik) equipped with a nitrogen laser (20 Hz) using settings and calibration as described [44,45]. FlexControl version 2.4 was used for instrument control, and FlexAnalysis version 2.4 for processing the data of the spectra. Annotated spectra were further analyzed by using the program BioTools 3.0 (Bruker Daltonik).

Cell binding and proliferation assays

Neuroblastoma cells (strain SK-N-MC) were cultured at 37°C in Eagle'sminimal essential medium with 10% fetal calf serum (Thermo Fischer Scientific, Dreieich, Germany) and non-essential amino acids in an atmosphere of 95% air and 5% CO_2. Cells grown to confluency in 96-well tissue culture plates for five days (~10^5 cells/well) were incubated for 16 h in medium without fetal calf serum. For the binding assays, serum-free Eagle's minimal essential medium (100 μl/well) with 25 mm HEPES, pH 7.4, 0.01% bovine serum albumin was used to block protein-binding sites, and the labeled galectins (specific radioactivities (150 kBq/μg for galectin-7 and 144 kBq/μg) at non-saturating concentrations. Protein iodination, measurement of carbohydrate-inhibitable binding of ^{125}I-labelled Gal-7 proteins to the cultured cells and data processing followed an optimized procedure [46].

Cell proliferation in the presence or absence of a Gal-7 protein was examined in 96-well tissue plates (Greiner, Nürtingen, Germany) by culturing cells in 100 μl medium for 48 h at 37°C and measuring cell growth with a cell proliferation kit (CellTiter-96, Promega, Heidelberg, Germany), as described previously [47,48]. The effect of the presence of 25 μg cholera toxin B-subunit (Ctx-B; Sigma) was examined after co-incubation with the tested galectin [47,48].

Results

Cis–trans isomerization at P4 reflected in HSQC spectra

The occurrence of two sets of resonances for distinct amino acids of Gal-7 is exemplified in the HSQC expansion in Figure 1A. It identifies doubled resonances arising from G124, G125, I13 and R31. For the most part,

Biochemical Journal (2020) **477** 3147–3165
https://doi.org/10.1042/BCJ20200499

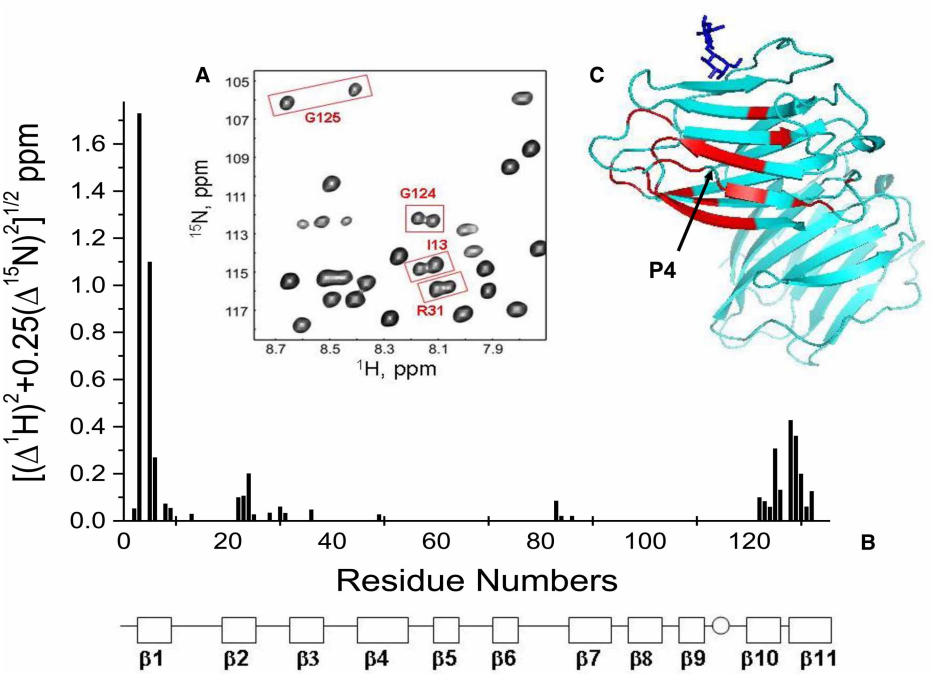

Figure 1. HSQC spectra of Gal-7 showing resonance doubling.

(**A**) Expansion of a ^{15}N–^{1}H HSQC spectrum of Gal-7 with some doubled resonances boxed in and labeled, as discussed in the text. (**B**) ^{15}N–^{1}H-weighted chemical shift differences, Δδ, between cross peak pairs are plotted vs. the amino acid sequence of Gal-7. The 11 β-strands in Gal-7 are identified at the bottom of the figure. (**C**) The structure of Gal-7 (PDB access code 4GAL) highlights in red residues showing doubled resonances. A molecule of bound lactose is shown in dark blue for structural orientation.

these resonance pairs originate from amino acids at the N- and C-termini that involve β-strands 1, 10 and 11 as well as from residues of proximal β-strands and loops at one side of the β-sandwich. In addition, a few more come from distinct sets of other amino acids, i.e. N36 (β-strand 3), L49 (β-strand 4) as well as R83, G84 and F87 (loop 6 between β-strands 6 and 7). These moieties are in close vicinity to the β-strands 2 and 10. All of the observed doubled resonances are documented in Figure 1B, where ^{15}N–^{1}H-weighted chemical shift differences, $\Delta\delta$, between cross peak pairs are plotted vs. the amino acid sequence of Gal-7. The residues are highlighted in the crystal structure in one of the subunits of the Gal-7 homodimer (PDB 4GAL), graphically providing an overview on the sites affected (Figure 1C).

To exclude the presence of a post-translational modification in at least a part of the protein fraction as cause for this phenomenon, Gal-7 was rigorously tested by MALDI-TOF mass spectrometry. As shown in Supplementary Figure S1, the peaks of both recombinant Gal-7 produced with regular and with ^{15}N-labeling media appear at the position calculated for unmodified Gal-7 and at 15 120 Da for the ^{15}N-labeled protein. Since the total number of nitrogen atoms in Gal-7 is 201, a complete labeling would produce a mass of 15 146 Da. Thus, extent of labeling reached ∼87% efficiency. The ensuing peptide mass fingerprinting adds validity to this result. Calculated and experimentally determined values (at a sequence coverage of 91.1% (regular) and 83% (^{15}N-labeled)) agreed with each other well (Supplementary Figure S2). The spectral resolution revealed an expectable heterogeneity due to different isotopic abundance (Supplementary Figure S3). These data confirm and extend (to the level of peptide fingerprinting) the initial observation of the absence of any modification for recombinant Gal-7 by electrospray ionization mass spectrometry [23]. This definitive evidence directs attention to examining the possibility of the presence of two different conformations resulting from peptide bond isomerization.

As illustrated in Figure 1A, the two resonances in each pair are in slow exchange so that the energy barrier between two conformational states must be quite high and cannot be attributed to differences in rapid internal motions. With this in mind, the most acceptable explanation is a *cis/trans*-isomerization at a proline moiety

Biochemical Journal (2020) **477** 3147–3165
https://doi.org/10.1042/BCJ20200499

that manifests a slow exchange on the chemical shift time scale, and the data on affected residues given above guided the search using human Gal-7's crystal structure to trace an elicitor [52]. Fittingly, one proline is positioned at the center of the group of residues, whose resonances undergo resonance doubling, i.e. the one at position 4 (labeled P4 in Figure 1C). We tested this proposal of involvement of such a process by engineering a site-specific Gal-7 mutant, in which P4 was replaced with a leucine to generate the P4L mutant that should adopt a single stable conformational state. Supplementary Figure S4 compares HSQC spectra of ^{15}N-labeled P4L mutant (red peaks) and ^{15}N-labeled wild-type Gal-7 (black peaks). A few regions where doubled signals were previously observed, are boxed in to show that these have been converted to single peaks. This comparison demonstrates that doubled peaks are no longer present in the HSQC spectrum of the P4L mutant, demonstrating that the observed conformational change in wild-type Gal-7 rests in *cis–trans* isomerization at P4, the stereochemistry at this site acting as a molecular switch.

For insight into this isomerization process, we next assigned each resonance in a pair to either the *cis* or the *trans* configuration at this position. At first, we grouped resonances in each pair by making sequence-specific assignments using HNCACB data. Results of this approach are illustrated in Figure 2A,B. These panels show strip plots for the selected amino acid sequence from E122 to V127. They disclose that G124, G125 and D126, each showing doubled resonances, can be grouped as labeled. At this point, we could only refer to these

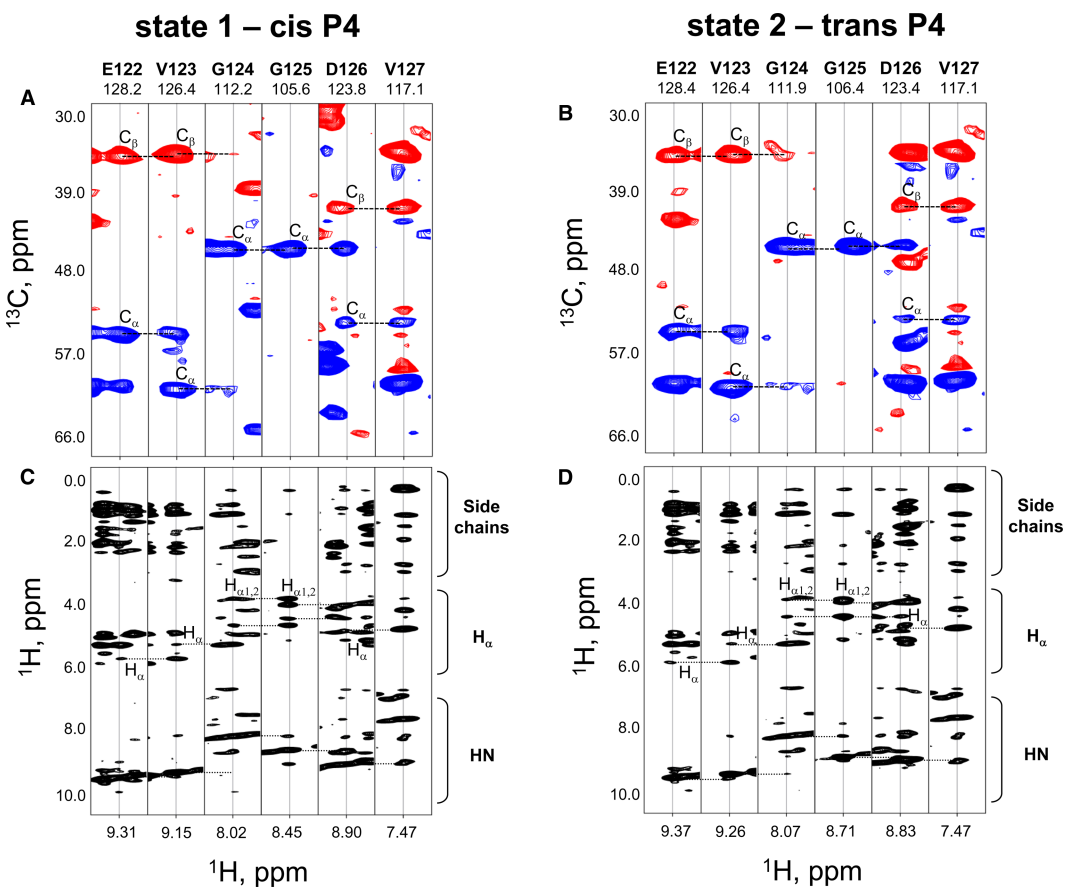

Figure 2. HNCACB spectra used for resonance assignments.

(**A**,**B**) Strip plots from an HNCACB experiment taken at the amide ^{15}N and ^{1}H chemical shifts of residues E122-V127 are shown for conformational states 1 (*cis* P4, **A**) and 2 (*trans* P4, **B**), as discussed in the text. Chemical shifts of C_α (blue cross-peaks) and C_β (red cross-peaks) atoms are indicated on the vertical axis. Horizontal dotted lines indicate sequential connectivity. (**C**,**D**) Strip plots from a ^{15}N-HSQC-NOESY experiment taken at the amide ^{15}N and ^{1}H chemical shifts of the same residues as in panels (**A**) and (**B**) for Gal-7 P4 cis (**C**) and trans (**D**) states. ^{1}H chemical shifts are indicated on the vertical axis, and horizontal dotted lines show sequential connectivity.

Biochemical Journal (2020) **477** 3147–3165
https://doi.org/10.1042/BCJ20200499

Table 1. Resonance assignments for residues showing doubled resonances due to *trans*- and *cis*- at P4

	P4 *trans*-state		P4 *cis*-state	
	^{1}H	^{15}N	^{1}H	^{15}N
3	8.3368	122.8398	7.92864	115.9922
5	8.83915	120.9279	9.30426	124.5026
6	7.9543	125.2998	8.01535	126.4543
13	8.14318	114.7628	8.18224	114.9321
22	8.55584	125.8294	8.65653	125.8342
23	6.98164	110.024	6.93921	109.6225
25	7.81349	126.8022	7.77497	126.9239
25	7.81349	126.8022	7.77497	126.9239
28	8.00783	112.7664	7.95931	112.6913
30	9.77288	116.5473	9.82884	116.5161
31	8.1364	116.2752	8.09591	116.1814
83	8.55182	112.3722	8.45364	112.3079
86	8.47241	115.4363	8.50488	115.4729
121	8.84909	123.6155	9.39105	128.3833
123	9.20225	126.4689	9.28112	126.3715
124	8.14937	112.3163	8.09373	112.4715
125	8.67174	106.1385	8.41869	105.4444
126	8.83	123.4	8.9	123.8
127	7.49584	117.1904	7.49584	117.1904
128	8.00277	125.4523	8.11128	127.0734
129	8.7866	125.9289	8.96463	127.1541
130	9.022	125.5756	8.98959	124.889
132	8.27756	122.7921	8.2541	122.3009

groupings as state 1 and state 2. Assignment of the two states to the peptide bond toward P4 in either the *cis* or the *trans*-state was then done by determining chemical shifts of P4-derived resonances in HNCACB spectra and by analyzing ^{13}C-edited and ^{15}N-edited NOESY data in detail. For example, in the *trans*-isomer of this peptide bound, relatively strong NOEs were observed between P4 δH_2 and V3 αH (and βH_2) resonances (i.e. $C\alpha^{i-1}H\alpha^{i-1}/C\delta^{i}H\delta^{i}$), whereas NOEs were detected between the P4 αH and V3 αH resonances (i.e. $C\alpha^{i-1}H\alpha^{i-1}/C\alpha^{i}H\alpha^{i}$) in the *cis*-state. In addition, the following parameter could be exploited for reaching a definitive assignment: ^{13}C chemical shifts for P in both configurations are known to differ significantly, especially the chemical shift difference between $^{13}C\beta$ and $^{13}C\gamma$ groups, as already documented in great detail [53–57]. Analyzing our respective NMR data accordingly allowed us to make isomer state-specific assignments for the resonances in each pair, which are listed in Table 1. The validity of these assignments is supported by examining intensities for resonances within each pair and comparing them with the expectable result. As previously reported, the *trans*-isomer state is normally the more populated one [58], and resonances listed for the *trans*-state in Table 1 were indeed observed as such.

Structure and dynamics of the two isomer states at P4

The NMR solution structure of Gal-7 was determined by using ^{15}N- and ^{13}C-edited NOESY, $^{3}J_{NH}$ coupling constants for dihedral angles, RDCs and the chemical shift index, as well as HD exchange and NH temperature factors to identify likely hydrogen bonds. Strip plots from ^{15}N-edited NOESY spectra for Gal-7 *cis* and *trans* states at P4 are exemplified and compared in Figure 2C,D, respectively. The set of inter-residue NOEs from either P4 isomer state is essentially the same, with generally lower NOE intensities for residues around P4 in

PORTLAND PRESS

Biochemical Journal (2020) **477** 3147–3165
https://doi.org/10.1042/BCJ20200499

Table 2. Structural statistics for NMR solution structures of Gal-7 in the P4 *cis*-state in the absence (apo-Gal-7) and presence of lactose (10 mM, holo-Gal-7)

Parameter	apo-Gal-7	holo-Gal-7
Constraints per monomer		
Intramolecular		
NOE distance restraints (total)	1659	1688
Average number of NOE restraints per residue	12	12
Long-range ($\|i–j\| > 4$)	511	525
Hydrogen bonds	69	69
RDC	67	67
Dihedral angle restraints	131	131
Intermolecular		
NOE distance restraints (total)	18	Interface: 24 Gal-7/lactose: 10
Hydrogen bonds	6	6
Ramachandran statistics		
Most-favorable region (%)	80.7	73.7
Additionally allowed region (%)	16.7	23.2
Generously allowed region (%)	2.2	2.2
Disallowed region (%)	0.4	0.9
RMSD to the mean structure for the backbone atoms (Å)	0.6	0.8
RMSD to the mean structure for non-hydrogen atoms (Å)	1.12	1.45

Structural statistics are essentially the same for Gal-7 in the P4 *trans*-state, albeit with several fewer NOEs and other constraints observed for N-terminal residues through L9.

the *trans*-state. Supplementary Figure S5A shows the temperature dependence of NH resonances in HSQC spectra acquired from 278 to 313 K, with some expansions provided in Supplementary Figure S5B–D. In either P4 isomer state, most resonances are shifted to the same extent, indicating the same potential to form hydrogen bonds. One clear exception is G125 (Supplementary Figure S5A boxed and S5B expanded), in which the signal for G125 NH in the *trans*-state changes little over this temperature range with a temperature factor of −2.2 ppb/K. In contrast, G125 NH in the *cis*-state exhibits a temperature factor of −6.8 ppb/K. In this regard, G125 in the *trans*-state is most probably involved in a hydrogen bond, whereas it is not in the *cis*-state. For the most part, NHs of the protein backbone that were identified as forming hydrogen bonds are correlated with β-strands involved in antiparallel β-sheet structures.

Using these NMR data, we calculated structures for Gal-7 in the *cis*- and *trans*-states at P4. Structural statistics are summarized in Table 2. Because Gal-7 is mostly dimeric at 400 μM [23,33,59] and HSQC data show the presence of only one set of resonances, the Gal-7 dimer in solution is symmetric as previously reported for the crystal structure of this lectin [52] (PDB code 4GAL). Because of this, we initially forced the Gal-7 dimer to remain symmetric during structural calculations. Moreover, several NOEs were observed between subunits, and this set of inter-subunit NOEs served as evidence for a single type of dimer being formed in either P4 isomer state. The 10 lowest energy-minimized Gal-7 structures out of 100 calculated exhibited root-mean-square deviations from the average structure of ∼0.6 Å for the β-sheet backbone Cα atoms and ∼1.1 Å for all non-hydrogen atoms (Table 2). The Cα traces of β-sheet-aligned structures for the apo-Gal-7 *cis*-state at P4 are superimposed in Figure 3A, along with a ribbon structure representation of the average structure in Figure 3B. Looking at the *cis*-based conformer, the hydrogen bond between N2 and G125 cannot form, consistent with the large negative NH temperature factor observed for Gal-7 in the P4 *cis*-state. However, the presence of more NOEs between N-terminal residues (residues 1–5) and the CRD β-sandwich in the P4 *cis*-state indicates that the N-terminus in the *cis*-state is more structurally integrated than in the *trans*-state. Aside from this N-terminal segment, the

Biochemical Journal (2020) **477** 3147–3165
https://doi.org/10.1042/BCJ20200499

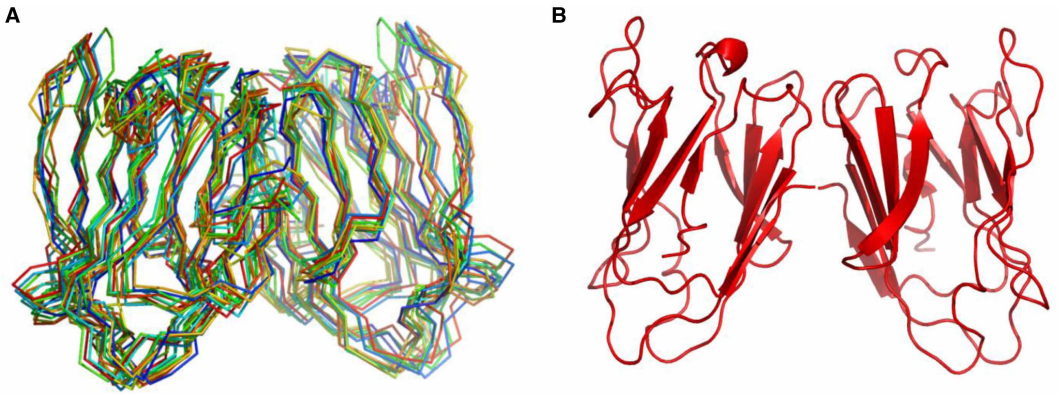

Figure 3. NMR-based structures of Gal-7.
Superpositions of the ten lowest energy structures (C_α traces) are shown for lactose-free apo-Gal-7 dimer (**A**), along with the average structure of this Gal-7 dimer in Pymol ribbon format (**B**).

structures of Gal-7 in the *cis*- and *trans*-states at P4 are the same, and thus only the P4 *cis*-state is shown in Figure 3. In addition, our NMR solution structure of Gal-7 is the same as that reported for the crystal structure of the lectin [52] (PDB code 4GAL, backbone RMSD < 1 Å) in which P4 is in the *trans*-state in both subunits of the dimer.

Because our Gal-7 structure is the same as those previously published, we focused attention on assessing internal motions of the backbone in Gal-7 P4 isomer states by using $^{1}H–^{15}N$ NMR relaxation data (T_1, T_2 and NOE) at 600 and 800 MHz and the Lipari–Szabo model free approach [43] to derive motional order parameters, S^2, for all NH vectors. Figure 4A,B shows plots of S^2 values for P4 *trans*- and *cis*-states vs. the amino acid sequence. Since average order parameters in both isomer states fall within the canonical range of 0.84–0.86, transient formation of Gal-7 dimers did not influence relaxation terms [60]. In general, backbone NH groups within β-strands are the most motionally restricted, whereas those at the N-terminus are relatively more mobile. On the other hand, C-terminal residues in β-strand 11, which is positioned behind the more mobile N-terminal β-strand-1, are relatively motionally restricted. Although trends in S^2 are generally the same for residues in the *trans*- and -*cis* states at P4, there are significant differences as shown in Figure 4C that plots ΔS^2 (*trans*-minus-*cis*) vs. the Gal-7 sequence. These data indicate that when P4 is in the *cis*-state, residues 3–6, 22–36 and 122–136 are more motionally restricted than they are in the *trans*-state. This observation is consistent with increased folding interactions between the N-terminus in the P4 *cis*-state and the main body of the CRD (see Figure 1).

Holo-Gal-7: structure, dynamics and lactose affinity

As with apo-Gal-7, we also collected NMR data on lactose-loaded Gal-7 (i.e. ^{15}N- and ^{13}C-edited NOESY, $^{3}J_{NH}$ coupling constants, chemical shift index and HD exchange). With the exception of chemical shifts of residues at the lactose binding site, the set of inter-residue NOEs, $^{3}J_{NH}$ coupling constants and HD exchange parameters were effectively the same for apo- and holo-Gal-7 in both P4 isomer states. Because of this, calculated structures for holo-Gal-7 varied little from those of apo-Gal-7. Structural statistics for holo-Gal-7 (Table 2), however, indicate that the calculated structure for apo-Gal-7 is somewhat better defined than that for holo-Gal-7. The reason for this apparently rests in differences in structural dynamics, with holo-Gal-7 exhibited greater internal mobility as observed for Gal-1 [62].

Lipari–Szabo model free analysis [43] of $^{1}H–^{15}N$ NMR relaxation data (T_1, T_2 and NOE) with lactose-loaded Gal-7 yielded motional order parameters, S^2, for all NH vectors. Plots of S^2 values for lactose-free and -loaded Gal-7 vs. the amino acid sequence of Gal-7 are shown in Figure 5A,B. Whereas trends in S^2 values for holo-Gal-7 parallel those for apo-Gal-7, there are differences as shown in Figure 5C, with alterations highlighted in color on the Gal-7 structure in Figure 5D (red and pink for increased mobility, and blue and cyan for decreased mobility). Note that the binding of lactose to Gal-7 generally increases backbone mobility throughout the structure, with the exception of residues at the lactose binding site itself. This observation is the

Biochemical Journal (2020) 477 3147–3165
https://doi.org/10.1042/BCJ20200499

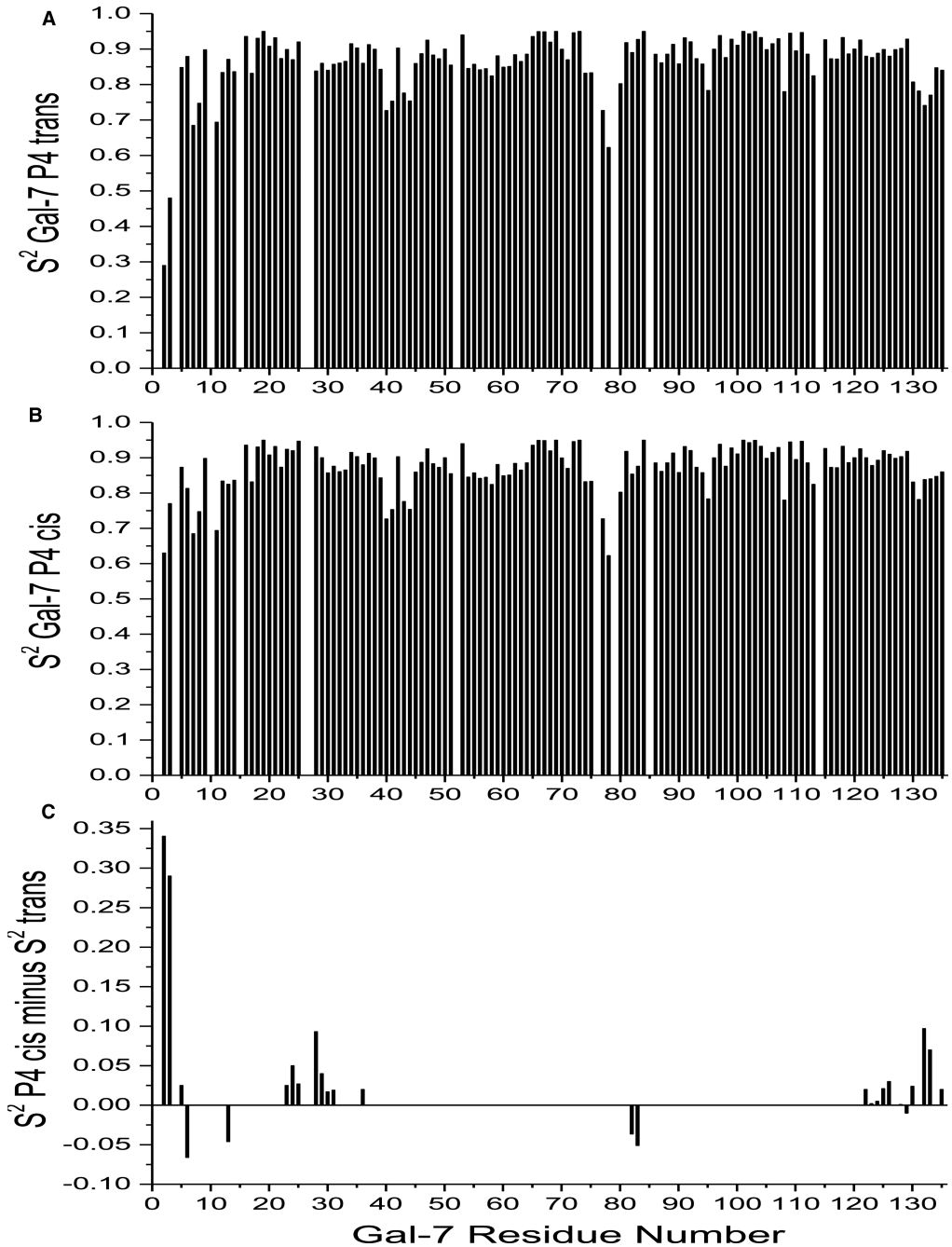

Figure 4. Motional order parameters derived from NMR relaxation data.

Internal motions in Gal-7 conformational states were assessed by acquiring $^{1}H–^{15}N$ NMR relaxation data (T_1, T_2 and NOE) at 600 and 800 MHz, and were analyzed by using the Lipari–Szabo model free approach [43] to derive motional order parameters, S^2, for all NH vectors. (**A**) S^2 values for P4 *trans*-state vs. the amino acid sequence. (**B**) S^2 values for P4 *cis*-state vs. the amino acid sequence. (**C**) ΔS^2 values (*trans*-minus-*cis*) vs. the Gal-7 sequence showing that differences are primarily localized around P4 and the P4 *cis*-state is more motionally restricted.

same as that found with Gal-1 [62]. Using equations reported previously that relate changes in S^2 to conformational entropy, ΔS [61], we find that, for lactose binding to Gal-7, $\Delta S/k$ is +0.1/residue. In regions with the largest differences in S^2, $\Delta S/k$ increases to +0.18/residue. Residues within and around the lactose-binding site

Biochemical Journal (2020) **477** 3147–3165
https://doi.org/10.1042/BCJ20200499

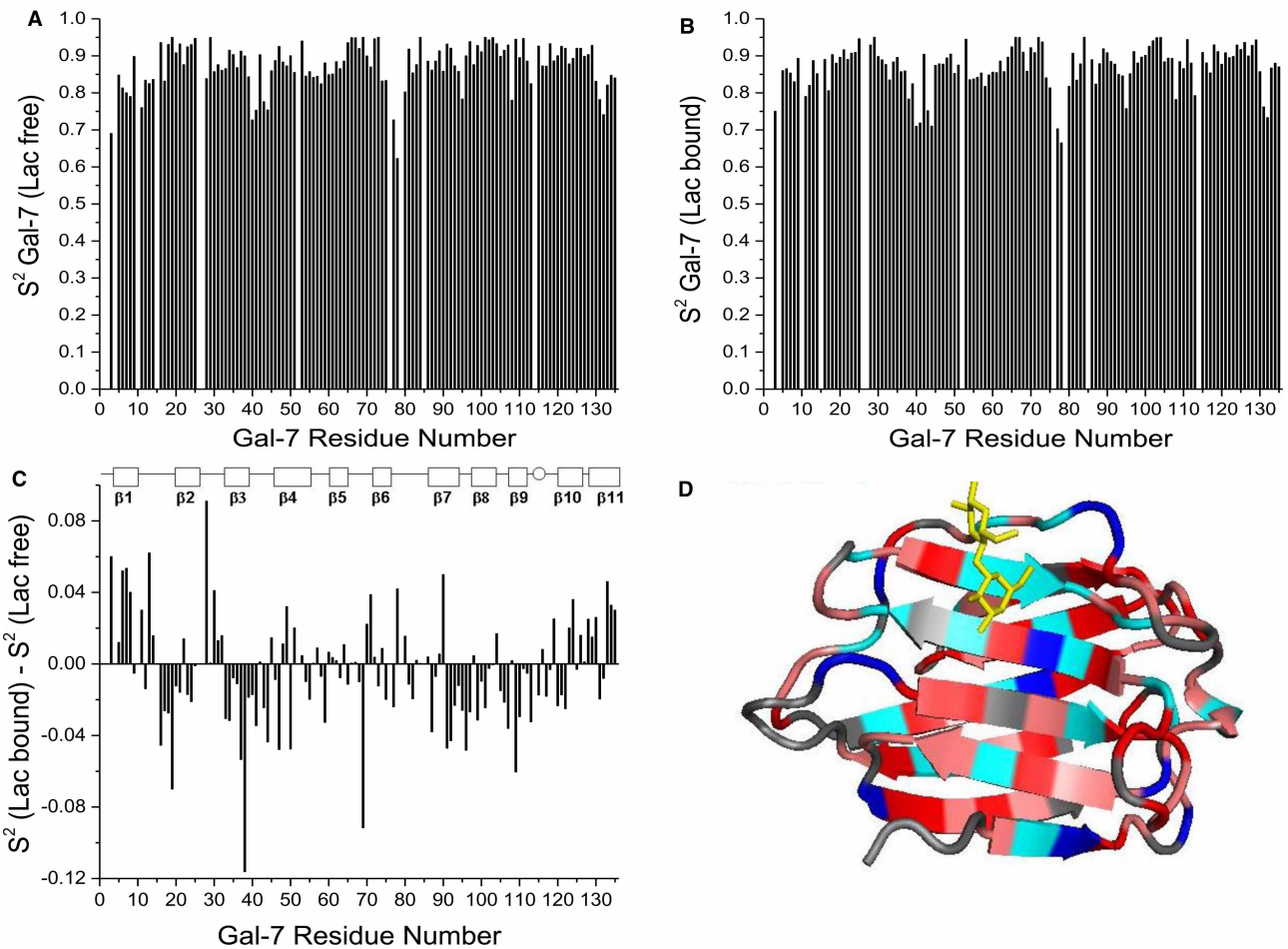

Figure 5. NMR-derived motional order parameters.

Order parameters, S^2, for lactose-free (**A**) and lactose-loaded (**B**) Gal-7 P4 *trans*-states vs. the amino acid sequence. (**C**) The difference in order parameters, ΔS^2 [calculated as S^2 for lactose-free minus S^2 for lactose-loaded protein] is shown vs. the Gal-7 amino acid sequence. These terms were derived from T_1 and T_2 relaxation times and NOE values determined at 600 and 800 MHz and analyzed by using the Lipari–Szabo model free approach as discussed in the text. A positive ΔS^2 value indicates more restricted motion for an NH vector of that residue in the lactose bound state, and a negative ΔS^2 value indicates less restricted motion for an NH vector in that residue in the lactose bound state. (**D**) Crystallographic structure of Gal-7 (PDB access code 4GAL) highlights differences shown in panel (**C**), with negative ΔS^2 values highlighted in shades of red and positive ΔS^2 values highlighted in shades of blue. Gray indicates not significant change. A molecule of bound lactose is shown in yellow for structural orientation.

and of the N- and C-termini are exceptions, where $\Delta S/k$ is −0.07/residue and −0.09/residue, respectively. As noted previously with Gal-1 [62], conformational entropy of the lectin is increased upon ligand binding, and thus contributes to a positive entropy term (ΔS) to reduce the extent of entropic penalty within the enthalpy-driven process of lactose binding, as reported by isothermal titration calorimetry for Gal-7 testing di-, tetra- and hexasaccharides (N-acetyllactosamine and its di- and trimers), as well as for the glycoprotein asialofetuin [63,64].

Having identified *cis/trans*-isomerization at P4 to generate two Gal-7 conformers in slow exchange on the NMR chemical shift time scale, we could refine analysis of ligand binding by this lectin in two structural states. Previously, we reported that lactose binds to Gal-7 with positive cooperativity [33], where the first step has an equilibrium association binding constant (K_1) of $4 \pm 2 \times 10^3\ M^{-1}$, followed by association of the second lactose molecule with $K_2 = 17 \pm 7 \times 10^3\ M^{-1}$, and this by looking at signals for the *trans*-state conformer. Here, we found that the affinity of lactose for the Gal-7 P4 *cis*-state is the same as that for the *trans*-state, with either state exhibiting positive cooperativity in ligand binding. This indicates that P4 *cis/trans*-isomerization has no

Biochemical Journal (2020) 477 3147–3165
https://doi.org/10.1042/BCJ20200499

significant effect on affinity for the canonical glycan ligand. By performing a titration with lactose on the Gal-7 P4L mutant, we also found no significant difference in affinity constants for lactose binding of Gal-7 as a single conformer (data not shown).

Cell binding and growth-inhibitory activity of wild-type Gal-7 and its P4L mutant

Having analyzed lactose binding to wild-type Gal-7 and its P4L mutant, we addressed the question of whether removal of the P4 conformational switch affects binding to a physiological glycan counter-receptor in cell assays. Based on our previous observation that Gal-7 is a receptor for the pentasaccharide of ganglioside GM1 for differentiating human neuroblastoma (SK-N-MC) cells and that this pairing induces growth inhibition [23], we performed a Scatchard analysis of glycan-inhibited cell-surface binding using radio-iodinated wild-type Gal-7 and its P4L mutant. The interaction of GM1 with human galectins has been thoroughly characterized in solution and *in silico* by docking analysis. The evidence that GM1 is a counter-receptor for galectins on human neuroblastoma (SK-N-MC) cells has been extended to Gal-7, and the application of a so-called neoganglio-protein presenting the GM1 lysoganglioside on albumin demonstrated the physical interaction of Gal-7 with GM1 in a carbohydrate-inhibitable manner with a K_D-value of 2.29 ± 1.27 μM [23] and to other members of the galectin family [46]. Thus, our Scatchard analysis determines the affinity of a proven cell surface-presented ligand. As shown in Figure 6A, the resulting affinity is 814 ± 152 nM for wild-type and 761 ± 121 nM for P4L, values that are similar. The presence of a ganglioside GM1 receptor, i.e. cholera toxin B-subunit, at 25 μg/ml reduced the extent of binding (Figure 6A, dashed lines), as target selection by Gal-7 in this cell system was expected.

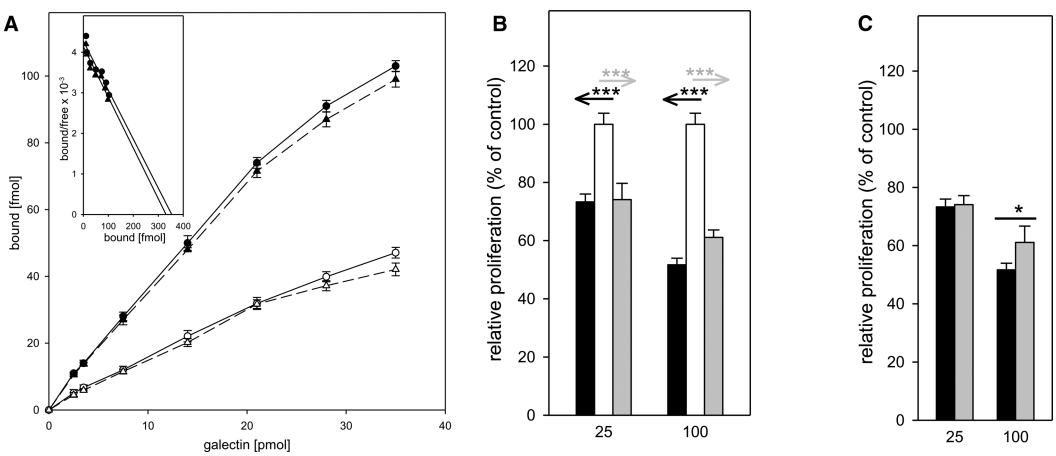

Figure 6. Effect of lectins on neuroblastoma cell growth.

(**A**) Binding of iodinated Gal-7-WT (●, solid line) and Gal-7-P4L (▲, solid line) to the surface of human neuroblastoma cells was quantitated for cells cultured in 96-well plates for five days (final density: 10^5 cells per well) prior to adding of the iodinated probe. Results are the means of three independent experiments ± SD. Binding was also measured in the presence of 0.25 mg/ml Ctx B: Gal-7-WT + Ctx (○, dashed line), Gal-7-P4L + Ctx B (Δ, dashed line). Inset, Scatchard plots. These experiments were performed in 96-well plates with 100 μl of medium. To display original results, the binding diagram shows the total amount of free ligand in 100 μl vs. the amount of ligand bound to cells. These data were used to calculate numbers for the Scatchard plot. Consequently, the K_D (that is read directly from the Scatchard plot) has the dimension of fmol/100 μl. However, to express the result as a molar concentration, we expanded this to fmol/l: fmol/100 μl = fmol × 10^4/100 μl × 10^4 = fmol/l. Since this resulted in relatively high values, we converted the molar concentration representing the K_D value to nM = nmol/l, that is nmol/l = fmol × 10^{-6}/l. (**B**,**C**) Effects of lectins on neuroblastoma cell growth were measured in proliferation assays after 48 h incubation in the presence of wild-type Gal-7 (black bar) or the P4L variant (gray bar), using untreated cultures in parallel as control, set to 100% and as reference (**B**). Statistical evaluation of the two data sets in direct comparison is given in (**C**). Results are the means of four independent experiments ± SD, level of significance is graded into three categories: * $0.05 \geq P > 0.01$, ** $0.01 \geq P \geq 0.005$ and *** $P < 0.005$.

Biochemical Journal (2020) 477 3147–3165
https://doi.org/10.1042/BCJ20200499

Next, we tested the two proteins for their effects on cell proliferation. Induction of growth inhibition was indistinguishable at 25 μg/ml, whereas the wild-type protein was more active than its P4L mutant at 100 μg/ml (Figure 6B,C). Although the affinity of cell binding was indistinguishable, the efficiency of blocking cell growth that depends on lattice formation on the cell surface at the higher concentration, appeared to be somewhat different, suggesting an impact of the mutation on characteristics and/or activity of surface cluster arrangements required to cause the experimental read-out.

Isomer states at P4 influence the Gal-7 monomer–dimer equilibrium

During this study, we observed a dependence of *cis/trans*-originating resonance intensities from P4 on the Gal-7 concentration. Figure 7A shows an HSQC spectrum of ^{15}N-labeled Gal-7 at 680 μM (black peaks) overlaid with that of Gal-7 at 40 μM (red peaks). At the higher Gal-7 concentration, resonance intensities of the *trans*- and *cis*-states (e.g. boxed G125 resonances at the top of the HSQC) are nearly equal. At the lower Gal-7 concentration, residues in the P4 *cis*-state display relatively greater resonance intensities. Figure 7B presents overlaid expansions of these HSQC spectra (boxed G125 resonances) at several Gal-7 concentrations. Figure 7C plots the change in ^{1}H (top panel) and ^{15}N (middle panel) chemical shifts vs. the Gal-7 concentration for the best-resolved signal, i.e. G125, of the *cis*- and *trans*-isomer pair. At Gal-7 concentrations less than ∼400 μM, chemical shifts and resonance intensities for these peaks changed significantly, with concentration-dependent changes correlated with the *trans/cis*-derived intensity ratio (Figure 7C, bottom panel). This trend demonstrates that the population of Gal-7 in the *cis*-state at P4 is increased at lower protein concentrations at the expense of its *trans*-isomer state. Since Gal-7 is a homodimer at high concentrations, this concentration-dependent trend indicates a shift in the monomer–dimer equilibrium to the monomer state at the lower Gal-7 concentrations.

At first, this observation was unexpected, because we previously derived K_d values for Gal-7 dimer dissociation of ∼2 μM using FPLC gel filtration data [33]. For further insight into this issue, we performed ^{15}N-edited PFG NMR experiments to determine the diffusion coefficient, *D*, as a function of Gal-7 concentration in the absence and presence of lactose (Figure 8). Dashed lines represent theoretical *D* values calculated using the Stokes–Einstein relationship [65]. At the highest Gal-7 concentrations, observed *D* values ($\sim 1.05 \times 10^{-6}$ cm^2/s) are the same as the theoretical *D* value for the dimer state. As the Gal-7 concentration is reduced in the absence of lactose (apo-Gal-7, black squares), the *D* value is increased, as expected upon dimer dissociation and increasing populations of the smaller sized monomer. From these NMR diffusion data, we estimate that the monomer–dimer equilibrium constant, K_d, for apo-Gal-7 is ∼19 μM, the concentration at which populations of monomer and dimer are about equal. Our NMR-derived K_d value falls between those of 30 μM derived using fluorescence resonance energy transfer (FRET) [33] and 10 μM derived using ultracentrifugation [23]. Moreover, the 50% dissociation point is about the mid-point in our plot of the *trans/cis* intensity ratio (Figure 7C, bottom panel), thus supporting the idea that Gal-7 monomers are favored when P4 is in its *cis*-state. Upon addition of lactose, the *D* value curve is shifted to lower Gal-7 concentrations (Figure 8), indicating greater stability of the Gal-7 dimer state and a shift to the *trans*-state at P4. This observation is consistent with our previous report that lactose binding stabilizes the Gal-7 dimer state [33]. Overall, our results indicate that isomerization at P4 affords the opportunity for Gal-7 to modulate its monomer–dimer equilibrium differently at low (probably physiological) concentrations.

Discussion

The possibility to adopt various conformations affords a versatile means to broaden a protein's range of functions. Structural conversions depend on some type of molecular on/off switching mechanism. In the case of lectins, the existence of two conformational states had first been reported with metal ion (Ca^{2+}, Mn^{2+}) binding to concanavalin A [66,67]. Instead of being involved in coordination bonding with the glycan [68], these metal ions induce a series of conformational changes that eventually shaped the contact site for the sugar by allowing the side chain of N208 to 'flop' into its appropriate position [69-71]. At the heart of this process was *trans*- to *cis*-isomerization of a non-prolyl peptide bond at A207-N208 that promoted cation binding. In a survey of a non-redundant set of 571 proteins, 12 of the 43 hits for non-proline peptide bonds in *cis*-configuration (often located close to the active site) were sugar receptors or carbohydrate-processing enzymes [72]. Among them is the lentil lectin LCA with its β-sandwich fold just like concanavalin A [73], and the snowdrop lectin GNA with its β-prism II fold [74].

Biochemical Journal (2020) **477** 3147–3165
https://doi.org/10.1042/BCJ20200499

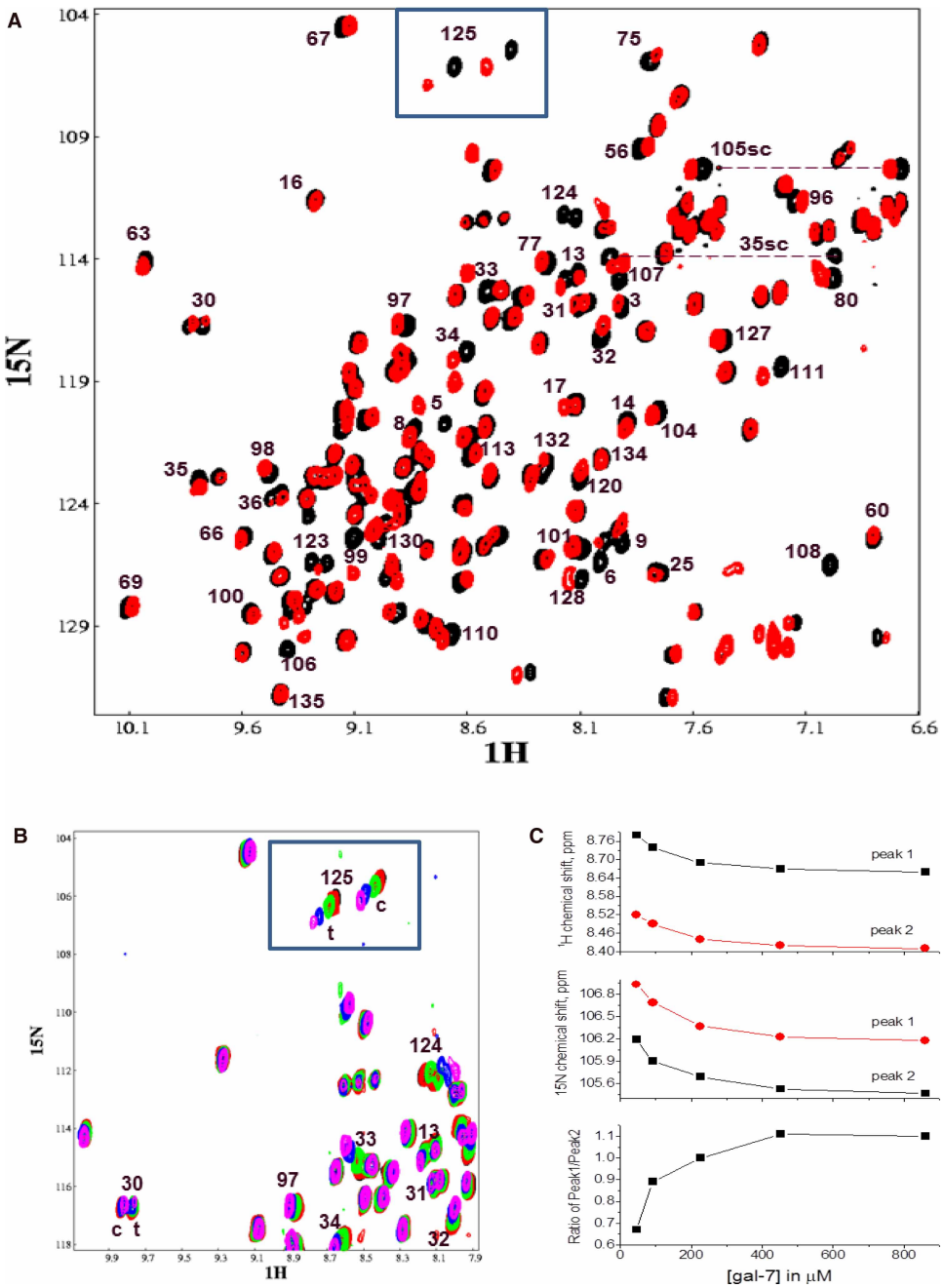

Figure 7. Effect of Gal-7 concentration on aggregate state.

(**A**) HSQC spectrum of ^{15}N-labeled Gal-7 at 680 μM (black peaks) overlaid with that of Gal-7 at 40 μM (red peaks). Some of the peaks are labeled with the Gal-7 sequence number. (**B**) Overlays of expansions from HSQC spectra acquired at several Gal-7 concentrations: 40 μM (black peaks), 100 μM (red peaks), 210 μM (green peaks), 425 μM (blue peaks), 850 μM (magenta peaks). (**C**) The change in ^{1}H (top panel) and ^{15}N (middle panel) chemical shifts vs. the Gal-7 concentration for the G125 *cis* (labeled peak 1) and *trans* (labeled peak 2) isomer pair. The *trans*/*cis* intensity ratio vs. Gal-7 concentration is shown in the bottom panel.

This phenomenon of shifting the position of a *trans*/*cis*-equilibrium in a peptide bond by a binding a divalent cation (or Tb^{3+}) had also been discovered for the rat liver and serum collecting mannose-binding protein A/C (MGP-A/C), two Ca^{2+}-dependent C-type lectins. In this case, however, proline (and its coordination with

Biochemical Journal (2020) **477** 3147–3165
https://doi.org/10.1042/BCJ20200499

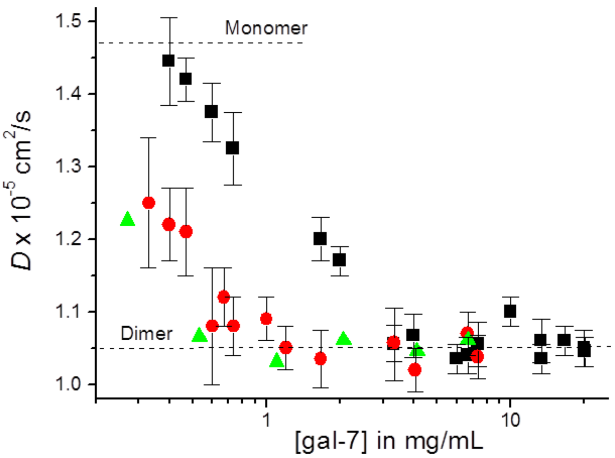

Figure 8. Molecular diffusion measured by PFG-NMR.

^{15}N-edited PFG NMR-derived diffusion coefficients, *D*, are plotted as a function of Gal-7 concentration in the absence of lactose (black squares) as well as in the presence of lactose at 10 mM (red circles) and at 25 mM (green triangles).

sugar) is involved. The cation-induced prolyl peptide bond isomerization at E190-P191 (P186 in MBP-A) allows these C-type lectins to preferentially adopt the active *cis*-form, whereas loss of the cation triggers a switch back to a ∼80–85% population of the *trans*-state which lacks the capacity to accommodate the cognate glycan [75,76]. In these two studies, the functionally intriguing opportunity to separate cargo from endocytic C-type lectins (which bear the highly conserved Pro residue at this strategic site) during endosomal transit upon exposure to an acidic pH that causes loss of Ca^{2+} (as suggested earlier [77], had not gone unnoticed. Keeping these precedents of Ca^{2+}-triggered (non)-prolyl peptide bond isomerization in leguminous (seed) and mammalian (C-type) lectins in mind, we formulated the basic question as to whether a prolyl peptide bond isomerization can occur in a human Ca^{2+}-independent lectin, thus establishing a putative molecular switch.

In our present study, we identified such a cation-independent process for a human galectin, namely position P4 of Gal-7. This discovery explained the occurrence of resonance pairs in NMR data of human Gal-7. Working with an engineered P4L mutant and acquiring NMR resonance assignments and inter-subunit NOEs, we found that the homo-dimeric lectin could exist as a mixed *cis/trans*-hetero-dimer. Lactose binding did not affect this equilibrium, with both conformations exhibiting rather equal affinities. If we assume functional relevance for this isomer generation, then this would imply an impact on activity other than glycan binding. Moreover, conformational changes occur at places away from the immediate vicinity of the lactose contact site that we defined in detail. For example, the N-terminus can move between a core-associated and a more solvent-exposed structure. Since shuttling between cellular compartments, as well as export, may involve this region as indicated with Gal-3 and its structural organization at this site [78,79], and N-terminal contact has been documented for Gal-1 around L11 in Ras-dependent growth regulation [80], tipping the balance toward one conformer or another here could be physiologically relevant, even providing a possible explanation for different intracellular routing of a galectin. Of note, the detected alterations go beyond the conformational repositioning at P4, as it affects the lectin more globally. As a consequence, this region of the protein (a platform for possible contacts with other proteins) can form two structures, each with its own complementarity profile.

In view of the capacity of Gal-7 to interact with key mediators of growth as mentioned in the introduction, mapping of the contact sites will thus be timely for counter-receptors in solution to trace respective pairing at this site. Conceptually, this has been done in this way for Gal-1 and the pre-B cell receptor. In this case, protein–protein interactions outside of the canonical lactose binding site, were depicted [81]. Also worth noting is that in the crystal structure of chicken galectin-1B (CG-1B), the proline residue at this analogous position in the *trans*-conformation (sandwiched by C2 and C7 that can form inter- and intra-subunit disulfide bridges) has been shown to stabilize the hydrophobic core at the interface [82], an indication for isomerization not yet studied. In addition to affecting interactions with protein counter-receptors and relative positions of members of the cysteine pair, this region around P4 at the interface could also regulate the extent of hetero-dimerization with subunits of other galectins, such as Gal-1 or -3, documented to occur recently [83]. When looking at galectin structures [84], crystallographic evidence for an isomerization at this site to the *cis*-state is available for

Biochemical Journal (2020) **477** 3147–3165
https://doi.org/10.1042/BCJ20200499

the Charcot–Leyden crystal protein [85] (termed Gal-10) despite a lack to bind the canonical glycan ligand lactose as is the case for the galectin-related protein [6,86]. The conservation of proline within the N-terminal stretch (albeit to a limited extent) and the difference with the analogous pair CG-1A/B (CG-1A and also human Gal-1 having a leucine rather than proline at the equivalent position) hypothetically indicate a possible relevance, thus warranting investigation with functional studies.

Overall, our report on the prolyl peptide isomerization at P4 in human Gal-7 raises the perspective to systematically explore this so far unrecognized phenomenon for galectins. This molecular process may provide dynamic structural flexibility for Gal-7 to adapt to a high-affinity, and even cross-linking, state from the mixed-conformer form of the homodimer upon association with non-glycan counter-receptors, and the observed difference in growth inhibition of neuroblastoma cells as a sign for a more active surface lattice at higher concentrations. Structural conversion then may bring about a similar outcome, as the presence of an N-glycan does, for a galectin, if directed to enter the endoplasmic reticulum [17]. Since galectins are at least bifunctional, they can engage in binding more than one partner. Cooperation between sites for glycan binding and for non-glycan contacts on the cell surface has been documented to occur with Ctx-B [87,88], providing us with an inspiring model, and, indeed, recently for Gal-3 when interacting with a glycan and the chemokine CXCL12 [89].

In this sense, our present data provide a clear direction for further research. Thus comparative assays with wild-type Gal-7 and its P4L mutant appear warranted, as generation of a change to the P4L status on the genome level is a new type of variant design for delineating structure-activity relationships [90,91]. In this context, we should note the occurrence of two Gal-7 genes in man and primates [92]. Equally relevant is the P-to-H substitution in mouse and rat Gal-7, a factor to note when extrapolating data across species barriers, that can prompt studies with variants bearing a proline at this site (with a mutant or with cells engineered to express the mutant lectin, in comparison with wild-type controls) and complement work with mutant(s) of human Gal-7. With these tools in hand, the next steps toward defining the biological relevance for this isomerization process (if any) can confidently be undertaken.

Competing Interests

The authors declare that there are no competing interests associated with the manuscript.

Funding

The author declares that there are no sources of funding to be acknowledged.

Authors Contribution

M.C.M., I.V.N., V.A.D. and H.I. performed the NMR experiments, and helped write the manuscript. M.C.M., I.V.N. and A.D. calculated the NMR-based structures and performed molecular dynamics studies. M.M. and J.K. performed the MS studies and helped write the manuscript. H.K. and H.J.G. expressed, isolated and purified the galectin proteins used in the study and helped write the manuscript. K.H.M. supervised the NMR work, analyzed and interpreted NMR data, and wrote the manuscript.

Acknowledgements

We are greatly indebted to Lieselotte Mantel for her excellent technical assistance. NMR Instrumentation was provided with funds from the NSF (BIR-961477), the University of Minnesota Medical School and the Minnesota Medical Foundation. The authors also wish to thank the Minnesota Supercomputing Institute (University of Minnesota) for providing computer resources. K.H.M. is also most grateful for financial support from the Ludwig-Maximillians-Universitaet Center for Advanced Study, and the Alexander von Humboldt Stiftung, during his 2019 sabbatical stay in Munich, Germany.

Abbreviations

CG, chicken galectin; CRD, carbohydrate recognition domain; Ctx-B, cholera toxin B-subunit; Gal-7, galectin-7; HDX, hydrogen-deuterium exchange; HSQC, heteronuclear single quantum coherence; NMR, nuclear magnetic resonance; NOESY, nuclear Overhauser effect spectroscopy; PFG, pulse field gradient.

References

1 Madsen, P., Rasmussen, H.H., Flint, T., Gromov, P., Kruse, T.A., Honoré, B. et al. (1995) Cloning, expression and chromosome mapping of human galectin-7. *J. Biol. Chem.* **270**, 5823–5829 https://doi.org/10.1074/jbc.270.11.5823

2 Lu, J., Pei, H., Kaeck, M. and Thompson, H.J. (1997) Gene expression changes associated with chemically induced rat mammary carcinogenesis. *Mol. Carcinog.* **20**, 204–215 https://doi.org/10.1002/(SICI)1098-2744(199710)20:2<204::AID-MC7>3.0.CO;2-M

3 Polyak, K., Xia, Y., Zweier, J.L., Kinzler, K.M. and Vogelstein, B. (1997) A model for p53-induced apoptosis. *Nature* **389**, 300–305 https://doi.org/10.1038/38525

4 Teichberg, V.I., Silman, I., Beitsch, D.D. and Resheff, G. (1975) A β-D-galactoside-binding protein from electric organ tissue of *Electrophorus electricus*. *Proc. Natl. Acad. Sci. U.S.A.* **72**, 1383–1387 https://doi.org/10.1073/pnas.72.4.1383

5 Hirabayashi, J. (1997) Recent topics on galectins. *Trends Glycosci. Glycotechnol.* **9**, 1–180 https://doi.org/10.4052/tigg.9.1

6 Cooper, D.N.W. (2002) Galectinomics: finding themes in complexity. *Biochim. Biophys. Acta* **1572**, 209–231 https://doi.org/10.1016/S0304-4165(02)00310-0

7 Kaltner, H., Toegel, S., García Caballero, G., Manning, J.C., Ledeen, R.W. and Gabius, H.-J. (2017) Galectins: their network and roles in immunity/tumor growth control. *Histochem. Cell Biol.* **147**, 239–256 https://doi.org/10.1007/s00418-016-1522-8

8 Hirabayashi, J. (2018) Special issue on galectins. *Trends Glycosci. Glycotechnol.* **30**, SE1–SE223 https://doi.org/10.4052/tigg.1736.1SJ

9 Gabius, H.-J. and Roth, J. (2017) An introduction to the sugar code. *Histochem. Cell Biol.* **147**, 111–117 https://doi.org/10.1007/s00418-016-1521-9

10 Kaltner, H., Abad-Rodríguez, J., Corfield, A.P., Kopitz, J. and Gabius, H.-J. (2019) The sugar code: letters and vocabulary, writers, editors and readers and biosignificance of functional glycan-lectin pairing. *Biochem. J.* **476**, 2623–2655 https://doi.org/10.1042/BCJ20170853

11 Liu, F.-T., Patterson, R.J. and Wang, J.L. (2002) Intracellular functions of galectins. *Biochim. Biophys. Acta* **1572**, 263–273 https://doi.org/10.1016/S0304-4165(02)00313-6

12 García Caballero, G., Schmidt, S., Schnölzer, M., Schlötzer-Schrehardt, U., Knospe, C., Ludwig, A.-K. et al. (2019) Chicken GRIFIN: binding partners, developmental course of localization and activation of its lens-specific gene expression by L-Maf/Pax6. *Cell Tissue Res.* **375**, 665–683 https://doi.org/10.1007/s00441-018-2931-x

13 Hughes, R.C. (1999) Secretion of the galectin family of mammalian carbohydrate-binding proteins. *Biochim. Biophys. Acta* **1473**, 172–185 https://doi.org/10.1016/S0304-4165(99)00177-4

14 Haudek, K.C., Spronk, K.J., Voss, P.G., Patterson, R.J., Wang, J.L. and Arnoys, E.J. (2010) Dynamics of galectin-3 in the nucleus and cytoplasm. *Biochim. Biophys. Acta* **1800**, 181–189 https://doi.org/10.1016/j.bbagen.2009.07.005

15 Funasaka, T., Raz, A. and Nangia-Makker, P. (2014) Nuclear transport of galectin-3 and its therapeutic implications. *Semin. Cancer Biol.* **27**, 30–38 https://doi.org/10.1016/j.semcancer.2014.03.004

16 Sato, S. (2018) Cytosolic galectins and their release and roles as carbohydrate-binding proteins in host-pathogen interaction. *Trends Glycosci. Glycotechnol.* **30**, SE199–SE209 https://doi.org/10.4052/tigg.1739.1SE

17 Kutzner, T.J., Higuero, A.M., Sussmair, M., Kopitz, J., Hingar, M., Diez-Revuelta, N. et al. (2019) How presence of a signal peptide affects human galectins-1 and -4: Clues to explain common absence of a leader sequence among adhesion/growth-regulatory galectins. *Biochim. Biophys. Acta* **1864**, 129449 https://doi.org/10.1016/j.bbagen.2019.129449

18 Kuwabara, I., Kuwabara, Y., Yang, R.Y., Schuler, M., Green, D.R., Zuraw, B.L. et al. (2002) Galectin-7 (PIG1) exhibits pro-apoptotic function through JNK activation and mitochondrial cytochrome c release. *J. Biol. Chem.* **277**, 3487–3497 https://doi.org/10.1074/jbc.M109360200

19 Saussez, S., Decaestecker, C., Lorfevre, F., Chevalier, D., Mortuaire, G., Kaltner, H. et al. (2008) Increased expression and altered intracellular distribution of adhesion/growth-regulatory lectins galectins-1 and -7 during tumour progression in hypopharyngeal and laryngeal squamous cell carcinomas. *Histopathology* **52**, 483–493 https://doi.org/10.1111/j.1365-2559.2008.02973.x

20 Cada, Z., Chovanec, M., Smetana, K., Betka, J., Lacina, L., Plzak, J. et al. (2009) Galectin-7: will the lectin's activity establish clinical correlations in head and neck squamous cell and basal cell carcinomas? *Histol. Histopathol.* **24**, 41–48 https://doi.org/10.14670/HH-24.41

21 Bernerd, F., Sarasin, A. and Magnaldo, T. (1999) Galectin-7 overexpression is associated with the apoptotic process in UVB-induced sunburn keratinocytes. *Proc. Natl. Acad. Sci. U.S.A.* **96**, 11329–11334 https://doi.org/10.1073/pnas.96.20.11329

22 Ueda, S., Kuwabara, I. and Liu, F.-T. (2004) Suppression of tumor growth by galectin-7 gene transfer. *Cancer Res.* **64**, 5672–5676 https://doi.org/10.1158/0008-5472.CAN-04-0985

23 Kopitz, J., André, S., von Reitzenstein, C., Versluis, K., Kaltner, H., Pieters, R.J. et al. (2003) Homodimeric galectin-7 (p53-induced gene 1) is a negative growth regulator for human neuroblastoma cells. *Oncogene* **22**, 6277–6288 https://doi.org/10.1038/sj.onc.1206631

24 Sturm, A., Lensch, M., André, S., Kaltner, H., Wiedenmann, B., Rosewicz, S. et al. (2004) Human galectin-2: novel inducer of T cell apoptosis with distinct profile of caspase activation. *J. Immunol.* **173**, 3825–3837 https://doi.org/10.4049/jimmunol.173.6.3825

25 Demers, M., Magnaldo, T. and St-Pierre, Y. (2005) A novel function for galectin-7: promoting tumorigenesis by up-regulating MMP-9 gene expression. *Cancer Res.* **65**, 5205–5210 https://doi.org/10.1158/0008-5472.CAN-05-0134

26 Campion, C.G., Labrie, M., Lavoie, G. and St-Pierre, Y. (2013) Expression of galectin-7 is induced in breast cancer cells by mutant p53. *PLoS One* **8**, e72468 https://doi.org/10.1371/journal.pone.0072468

27 Inagaki, Y., Higashi, K., Kushida, M., Hong, Y.Y., Nakao, S., Higashiyama, R. et al. (2008) Hepatocyte growth factor suppresses profibrogenic signal transduction via nuclear export of Smad3 with galectin-7. *Gastroenterology* **134**, 1180–1190 https://doi.org/10.1053/j.gastro.2008.01.014

28 Grosset, A.A., Labrie, M., Gagne, D., Vladoiu, M.C., Gaboury, L., Doucet, N. et al. (2014) Cytosolic galectin-7 impairs p53 functions and induces chemoresistance in breast cancer cells. *BMC Cancer* **14**, 801 https://doi.org/10.1186/1471-2407-14-801

29 Villeneuve, C., Baricault, L., Canelle, L., Barboule, N., Racca, C., Monsarrat, B. et al. (2011) Mitochondrial proteomic approach reveals galectin-7 as a novel bcl-2 binding protein in human cells. *Mol. Biol. Cell* **22**, 999–1013 https://doi.org/10.1091/mbc.e10-06-0534

30 Advedissian, T., Proux-Gillardeaux, V., Nkosi, R., Peyret, G., Nguyen, T., Poirier, F. et al. (2017) E-Cadherin dynamics is regulated by galectin-7 at epithelial cell surface. *Sci. Rep.* **7**, 17086 https://doi.org/10.1038/s41598-017-17332-y

31 Chen, H.L., Chiang, P.C., Lo, C.H., Lo, Y.H., Hsu, D.K., Chen, H.Y. et al. (2016) Galectin-7 regulates keratinocyte proliferation and differentiation through JNK-miR-203-p63 signaling. *J. Invest. Dermatol.* **136**, 182–191 https://doi.org/10.1038/JID.2015.366

32 Nesmelova, I.V., Berbis, M.A., Miller, M.C., Cañada, F.J., André, S., Jiménez-Barbero, J. et al. (2012) ^{1}H, ^{13}c, and ^{15}N backbone and side-chain chemical shift assignments for the 31kDa human galectin-7 (p53-induced gene 1) homodimer, a pro-apoptotic lectin. *Biomol. NMR Assign.* **6**, 127–129 https://doi.org/10.1007/s12104-011-9339-9

33 Ermakova, E., Miller, M.C., Nesmelova, I.V., Lopez-Merino, L., Berbís, M.A., Nesmelov, Y. et al. (2013) Lactose binding to human galectin-7 (p53-induced gene 1) induces long-range effects through the protein resulting in increased dimer stability and evidence for positive cooperativity. *Glycobiology* **23**, 508–523 https://doi.org/10.1093/glycob/cwt005

34 Nesmelova, I.V., Pang, M., Baum, L.G. and Mayo, K.H. (2008) ^{1}H, ^{13}c, and ^{15}N backbone and side-chain chemical shift assignments for the 29 kDa human galectin-1 protein dimer. *Biomol. NMR Assign.* **2**, 203–205 https://doi.org/10.1007/s12104-008-9121-9

35 Delaglio, F., Grzesiek, S., Vuister, G.W., Zhu, G., Pfeifer, J. and Bax, A. (1995) NMRPipe: a multidimensional spectral processing system based on UNIX pipes. *J. Biomol. NMR* **6**, 277–293 https://doi.org/10.1007/BF00197809

36 Johnson, B.A. (2004) Using NMRView to visualize and analyze the NMR spectra of macromolecules. *Methods Mol. Biol.* **278**, 313–352 https://doi.org/10.1385/1-59259-809-9:313

37 Chou, J.J., Delaglio, F. and Bax, A. (2000) Measurement of one-bond ^{15}N-^{13}C' dipolar couplings in medium sized proteins. *J. Biomol. NMR* **18**, 101–105 https://doi.org/10.1023/A:1008358318863

38 Nesmelova, I.V., Idiyatullin, D. and Mayo, K.H. (2004) Measuring protein self-diffusion in protein-protein mixtures using a pulsed gradient spin-echo technique with WATERGATE and isotope filtering. *J. Magn. Reson.* **166**, 129–133 https://doi.org/10.1016/j.jmr.2003.09.004

39 Nesmelova, I.V., Sham, Y., Dudek, A.Z., van Eijk, L.I., Wu, G., Slungaard, A. et al. (2005) Platelet factor 4 and interleukin-8 CXC chemokine heterodimer formation modulates function at the quaternary structural level. *J. Biol. Chem.* **280**, 4948–4958 https://doi.org/10.1074/jbc.M405364200

40 Daragan, V.A., Kloczewiak, M.A. and Mayo, K.H. (1993) ^{13}C nuclear magnetic resonance relaxation-derived (, (bond rotational energy barriers and rotational restrictions for glycine ^{13}C (-methylenes in a GXX-repeat hexadecapeptide. *Biochemistry* **32**, 10580–10590 https://doi.org/10.1021/bi00091a007

41 Idiyatullin, D., Krushelnitsky, A., Nesmelova, I., Blanco, F., Daragan, V.A., Serrano, L. et al. (2000) Internal motional amplitudes and correlated bond rotations in an α-helical peptide derived from^{13}C and ^{15}N NMR relaxation. *Protein Sci.* **9**, 2118–2127 https://doi.org/10.1110/ps.9.11.2118

42 Idiyatullin, D., Nesmelova, I., Daragan, V.A. and Mayo, K.H. (2003) Comparison of ^{13}CαH and ^{15}NH backbone dynamics in protein GB1. *Protein Sci.* **12**, 914–922 https://doi.org/10.1110/ps.0228703

43 Lipari, G. and Szabo, A. (1981) Nuclear magnetic resonance relaxation in nucleic acid fragments: models for internal motion. *Biochemistry* **20**, 6250–6256 https://doi.org/10.1021/bi00524a053

44 Kopitz, J., Vértesy, S., André, S., Fiedler, S., Schnölzer, M. and Gabius, H.-J. (2014) Human chimera-type galectin-3: defining the critical tail length for high-affinity glycoprotein/cell surface binding and functional competition with galectin-1 in neuroblastoma cell growth regulation. *Biochimie* **104**, 90–99 https://doi.org/10.1016/j.biochi.2014.05.010

45 García Caballero, G., Flores-Ibarra, A., Michalak, M., Khasbiullina, N., Bovin, N.V., André, S. et al. (2016) Galectin-related protein: an integral member of the network of chicken galectins. 1. From strong sequence conservation of the gene confined to vertebrates to biochemical characteristics of the chicken protein and its crystal structure. *Biochim. Biophys. Acta* **1860**, 2285–2297 https://doi.org/10.1016/j.bbagen.2016.06.001

46 Kopitz, J., von Reitzenstein, C., Burchert, M., Cantz, M. and Gabius, H.-J. (1998) Galectin-1 is a major receptor for ganglioside GM1, a product of the growth-controlling activity of a cell surface ganglioside sialidase, on human neuroblastoma cells in culture. *J. Biol. Chem.* **273**, 11205–11211 https://doi.org/10.1074/jbc.273.18.11205

47 Kopitz, J., von Reitzenstein, C., André, S., Kaltner, H., Uhl, J., Ehemann, V. et al. (2001) Negative regulation of neuroblastoma cell growth by carbohydrate-dependent surface binding of galectin-1 and functional divergence from galectin-3. *J. Biol. Chem.* **276**, 35917–35923 https://doi.org/10.1074/jbc.M105135200

48 Kopitz, J., Ballikaya, S., André, S. and Gabius, H.-J. (2012) Ganglioside GM1/galectin-dependent growth regulation in human neuroblastoma cells: special properties of bivalent galectin-4 and significance of linker length for ligand selection. *Neurochem. Res.* **37**, 1267–1276 https://doi.org/10.1007/s11064-011-0693-x

49 Schwieters, C.D., Kuszewski, J.J., Tjandra, N. and Clore, G.M. (2003) The Xplor-NIH NMR molecular structure determination package. *J. Magn. Reson.* **160**, 65–73 https://doi.org/10.1016/S1090-7807(02)00014-9

50 Dominguez, C., Boelens, R. and Bonvin, A.M. (2003) HADDOCK: a protein-protein docking approach based on biochemical or biophysical information. *J. Am. Chem. Soc.* **125**, 1731–1737 https://doi.org/10.1021/ja026939x

51 Phillips, J.C., Braun, R., Wang, W., Gumbart, J., Tajkhorshid, E., Villa, E. et al. (2005) Scalable molecular dynamics with NAMD. *J. Comput. Chem.* **26**, 1781–1802 https://doi.org/10.1002/jcc.20289

52 Leonidas, D.D., Vatzaki, E.H., Vorum, H., Celis, J.E., Madsen, P. and Acharya, K.R. (1998) Structural basis for the recognition of carbohydrates by human galectin-7. *Biochemistry* **37**, 13930–13940 https://doi.org/10.1021/bi981056x

53 Schubert, M., Labudde, D., Oschkinat, H. and Schmieder, P. (2002) A software tool for the prediction of Xaa-Pro peptide bond conformations in proteins based on ^{13}C chemical shift statistics. *J. Biomol. NMR* **24**, 149–154 https://doi.org/10.1023/A:1020997118364

54 Cavalli, A., Salvatella, X., Dobson, C.M. and Vendruscolo, M. (2007) Protein structure determination from NMR chemical shifts. *Proc. Natl. Acad. Sci. U.S.A.* **104**, 9615–9620 https://doi.org/10.1073/pnas.0610313104

55 Shen, Y., Lange, O., Delaglio, F., Rossi, P., Aramini, J.M., Liu, G. et al. (2008) Consistent blind protein structure generation from NMR chemical shift data. *Proc. Natl. Acad. Sci. U.S.A.* **105**, 4685–4690 https://doi.org/10.1073/pnas.0800256105

56 Shen, Y., Vernon, R., Baker, D. and Bax, A. (2009) De novo protein structure generation from incomplete chemical shift assignments. *J. Biomol. NMR* **43**, 63–78 https://doi.org/10.1007/s10858-008-9288-5

57 Wishart, D.S., Arndt, D., Berjanskii, M., Tang, P., Zhou, J. and Lin, G. (2008) CS23D: a web server for rapid protein structure generation using NMR chemical shifts and sequence data. *Nucl. Acids Res.* **36**, W496–W502 https://doi.org/10.1093/nar/gkn305

58 Wüthrich, K. (1986) *NMR of Proteins and Nucleic Acids*, John Wiley & Sons, New York

59 Morris, S., Ahmad, N., André, S., Kaltner, H., Gabius, H.-J., Brenowitz, M. et al. (2004) Quaternary solution structures of galectins-1, -3 and -7. *Glycobiology* **14**, 293–300 https://doi.org/10.1093/glycob/cwh029

60 Schurr, J.M., Babcock, H.P. and Fujimoto, B.S. (1994) A test of the model-free formulas. Effects of anisotropic rotational diffusion and dimerization. *J. Magn. Reson.* **105**, 211–224 https://doi.org/10.1006/jmrb.1994.1127

61 Prabhu, N.V., Lee, A.L., Wand, A.J. and Sharp, K.A. (2003) Dynamics and entropy of a calmodulin-peptide complex studied by NMR and molecular dynamics. *Biochemistry* **42**, 562–570 https://doi.org/10.1021/bi026544q
62 Nesmelova, I.V., Ermakova, E., Daragan, V.A., Pang, M., Menendez, M., Lagartera, L. et al. (2010) Lactose binding to galectin-1 modulates structural dynamics, increases conformational entropy, and occurs with apparent negative cooperativity. *J. Mol. Biol.* **397**, 1209–1230 https://doi.org/10.1016/j.jmb.2010.02.033
63 Ahmad, N., Gabius, H.-J., Kaltner, H., André, S., Kuwabara, I., Liu, F.-T. et al. (2002) Thermodynamic binding studies of cell surface carbohydrate epitopes to galectins-1, -3 and -7. Evidence for differential binding specificities. *Can. J. Chem.* **80**, 1096–1104 https://doi.org/10.1139/v02-162
64 Dam, T.K., Gabius, H.-J., André, S., Kaltner, H., Lensch, M. and Brewer, C.F. (2005) Galectins bind to the multivalent glycoprotein asialofetuin with enhanced affinities and a gradient of decreasing binding constants. *Biochemistry* **44**, 12564–12571 https://doi.org/10.1021/bi051144z
65 Cantor, C. R. and Schimmel, P. R. (1980) *Biophysical Chemistry*. pp. 1–3, Freeman, W. H., New York
66 Brown, III, R.D., Brewer, C.F. and Koenig, S.H. (1977) Conformation states of concanavalin A: kinetics of transitions induced by interaction with Mn^{2+} and Ca^{2+} ions. *Biochemistry* **16**, 3883–3896 https://doi.org/10.1021/bi00636a026
67 Koenig, S.H., Brewer, C.F. and Brown, III, R.D. (1978) Conformation as the determinant of saccharide binding in concanavalin A: Ca^{2+}-concanavalin A complexes. *Biochemistry* **17**, 4251–4260 https://doi.org/10.1021/bi00613a022
68 Gabius, H.-J. (2011) The how and why of Ca^{2+} involvement in lectin activity. *Trends Glycosci. Glycotechnol.* **23**, 168–177 https://doi.org/10.4052/tigg.23.168
69 Bouckaert, J., Loris, R., Poortmans, F. and Wyns, L. (1995) Crystallographic structure of metal-free concanavalin A at 2.5 Å resolution. *Proteins* **23**, 510–524 https://doi.org/10.1002/prot.340230406
70 Bouckaert, J., Poortmans, F., Wyns, L. and Loris, R. (1996) Sequential structural changes upon zinc and calcium binding to metal-free concanavalin A. *J. Biol. Chem.* **271**, 16144–16150 https://doi.org/10.1074/jbc.271.27.16144
71 Bouckaert, J., Dewallef, Y., Poortmans, F., Wyns, L. and Loris, R. (2000) The structural features of concanavalin A governing non-proline peptide isomerization. *J. Biol. Chem.* **275**, 19778–19787 https://doi.org/10.1074/jbc.M001251200
72 Jabs, A., Weiss, M.S. and Hilgenfeld, R. (1999) Non-proline *cis* peptide bonds in proteins. *J. Mol. Biol.* **286**, 291–304 https://doi.org/10.1006/jmbi.1998.2459
73 Loris, R., Van Overberge, D., Dao-Thi, M.H., Poortmans, F., Maene, N. and Wyns, L. (1994) Structural analysis of two crystal forms of lentil lectin at 1.8 A resolution. *Proteins* **20**, 330–346 https://doi.org/10.1002/prot.340200406
74 Hester, G., Kaku, H., Goldstein, I.J. and Wright, C.S. (1995) Structure of mannose-specific snowdrop *(Galanthus nivalis)* lectin is representative of a new plant lectin family. *Nat. Struct. Biol.* **2**, 472–479 https://doi.org/10.1038/nsb0695-472
75 Ng, K.K., Park-Snyder, S. and Weis, W.I. (1998) Ca^{2+}-dependent structural changes in C-type mannose-binding proteins. *Biochemistry* **37**, 17965–17976 https://doi.org/10.1021/bi981972a
76 Ng, K.K.-S. and Weis, W.I. (1998) Coupling of prolyl peptide bond isomerization and Ca^{2+} binding in a C-type mannose-binding protein. *Biochemistry* **37**, 17977–17989 https://doi.org/10.1021/bi9819733
77 Leitinger, B., Hille-Rehfeld, A. and Spiess, M. (1995) Biosynthetic transport of the asialoglycoprotein receptor H1 to the cell surface occurs via endosomes. *Proc. Natl. Acad. Sci. U.S.A.* **92**, 10109–10113 https://doi.org/10.1073/pnas.92.22.10109
78 Gong, H.C., Honjo, Y., Nangia-Makker, P., Hogan, V., Mazurak, N., Bresalier, R.S. et al. (1999) The NH_2 terminus of galectin-3 governs cellular compartmentalization and functions in cancer cells. *Cancer Res.* **59**, 6239–6245 PMID: 10626818
79 Flores-Ibarra, A., Vértesy, S., Medrano, F.J., Gabius, H.-J. and Romero, A. (2018) Crystallization of a human galectin-3 variant with two ordered segments in the shortened N-terminal tail. *Sci. Rep.* **8**, 9835 https://doi.org/10.1038/s41598-018-28235-x
80 Rotblat, B., Niv, H., André, S., Kaltner, H., Gabius, H.-J. and Kloog, Y. (2004) Galectin-1(L11A) predicted from a computed galectin-1 farnesyl-binding pocket selectively inhibits Ras-GTP. *Cancer Res.* **64**, 3112–3118 https://doi.org/10.1158/0008-5472.CAN-04-0026
81 Elantak, L., Espeli, M., Boned, A., Bornet, O., Bonzi, J., Gauthier, L. et al. (2012) Structural basis for galectin-1-dependent pre-B cell receptor (pre-BCR) activation. *J. Biol. Chem.* **287**, 44703–44713 https://doi.org/10.1074/jbc.M112.395152
82 López-Lucendo, M.F., Solís, D., Sáiz, J.L., Kaltner, H., Russwurm, R., André, S. et al. (2009) Homodimeric chicken galectin CG-1B (C-14): crystal structure and detection of unique redox-dependent shape changes involving inter- and intrasubunit disulfide bridges by gel filtration, ultracentrifugation, site-directed mutagenesis, and peptide mass fingerprinting. *J. Mol. Biol.* **386**, 366–378 https://doi.org/10.1016/j.jmb.2008.09.054
83 Miller, M.C., Ludwig, A.-K., Wichapong, K., Kaltner, H., Kopitz, J., Gabius, H.-J. et al. (2018) Adhesion/growth-regulatory galectins tested in combination: evidence for formation of hybrids as heterodimers. *Biochem. J.* **475**, 1003–1018 https://doi.org/10.1042/BCJ20170658
84 Kamitori, S. (2018) Three-dimensional structures of galectins. *Trends. Glycosci. Glycotechnol.* **30**, SE41–SE50 https://doi.org/10.4052/tigg.1731.1SE
85 Leonidas, D.D., Elbert, D.L., Zhou, Z., Leffler, H., Ackerman, S.J. and Acharya, K.R. (1995) Crystal structure of human Charcot-Leyden crystal protein, an eosinophil lysophospholipase, identifies it as a new member of the carbohydrate-binding family of galectins. *Structure* **3**, 1379–1393 https://doi.org/10.1016/S0969-2126(01)00275-1
86 Manning, J.C., García Caballero, G., Ruiz, F.M., Romero, A., Kaltner, H. and Gabius, H.-J. (2018) Members of the galectin network with deviations from the canonical sequence signature. 2. *G*alectin-*r*elated *p*rotein (GRP). *Trends Glycosci. Glycotechnol.* **30**, SE11–SE20 https://doi.org/10.4052/tigg.1727.1SE
87 Aman, A.T., Fraser, S., Merritt, E.A., Rodigherio, C., Kenny, M., Ahn, M. et al. (2001) A mutant cholera toxin B subunit that binds GM1- ganglioside but lacks immunomodulatory or toxic activity. *Proc. Natl. Acad. Sci. U.S.A.* **98**, 8536–8541 https://doi.org/10.1073/pnas.161273098
88 Rodighiero, C., Fujinaga, Y., Hirst, T.R. and Lencer, W.I. (2001) A cholera toxin B-subunit variant that binds ganglioside GM1 but fails to induce toxicity. *J. Biol. Chem.* **276**, 36939–36945 https://doi.org/10.1074/jbc.M104245200
89 Eckardt, V., Miller, M.C., Blanchet, X., Duan, R., Leberzammer, J., Duchene, J. et al. (2020) Chemokines and galectins form heterodimers to modulate inflammation. *EMBO Rep.* **21**, e47852 https://doi.org/10.15252/embr.201947852
90 Kaltner, H., García Caballero, G., Ludwig, A.-K., Manning, J.C. and Gabius, H.-J. (2018) From glycophenotyping by (plant) lectin histochemistry to defining functionality of glycans by pairing with endogenous lectins. *Histochem. Cell Biol.* **149**, 547–568 https://doi.org/10.1007/s00418-018-1676-7
91 Ludwig, A.-K., Kaltner, H., Kopitz, J. and Gabius, H.-J. (2019) Lectinology 4.0: altering modular (ga)lectin display for functional analysis and biomedical applications. *Biochim. Biophys. Acta* **1863**, 935–940 https://doi.org/10.1016/j.bbagen.2019.03.005
92 Kaltner, H., Raschta, A.-S., Manning, J.C. and Gabius, H.-J. (2013) Copy-number variation of functional galectin genes: studying animal galectin-7 (p53-induced gene 1 in man) and tandem-repeat-type galectins-4 and -9. *Glycobiology* **23**, 1152–1163 https://doi.org/10.1093/glycob/cwt052